INTERNATIONAL JOURNAL OF LATEST TECHNOLOGY IN ENGINEERING, MANAGEMENT & APPLIED SCIENCE (IJLTEMAS)

ISSN 2278-2540 | DOI: 10.51583/IJLTEMAS | Volume XIII, Issue III, March 2024

Assessment of the Quality of 17-4 PH Stainless Steel Scrap-Based Investment-Casting Turbine Blades for the Geothermal Turbine Component Application

***Agus Hadi Santosa Wargadipura[1], Razie Hanafi[1], Diah Ayu Fitriani[1], and Arli Guardi[2]**

[1]The Research Centre for Advanced Materials, National Research and Innovation Agency (BRIN),

[2]The Research Centre for Industrial Process and Manufacturing Technology, National Research and Innovation Agency (BRIN), KST BJ. Habibie, Puspiptek Serpong, Banten 15314, Indonesia

**Corresponding Author*

DOI: https://doi.org/10.51583/IJLTEMAS.2024.130306

Received: 10 January 2024; Accepted: 20 January 2024; Published: 03 April 2024

Abstract: This paper discusses an investigation of the ability of investment casting to manufacture rotor turbine blades using scrap materials. The manufacture of stainless steel of 17-4 PH is chosen to demonstrate alloying processes using the scrap materials. The alloying of stainless steel is performed using material balancing technique to match the standard chemical composition of stainless steel 17-4PH.The mechanical properties of the prototype of stainless steel 17-4PH is tested using the uniaxial tensile test machine to obtain the tensile stress and the Brinell impact test is carried out to evaluate the hardness of the material obtained. To evaluate the quality of the casting of the turbine blade obtained, the X-ray radiography of the turbine blade prototype is performed. The result obtained in this study shown that it is possible to have recycled stainless steel 17-4PH to be used in producing turbine blades.

Keywords: 17-4 PH stainless steel, precipitation hardening, char py impact, tensile strength, heat treatment, X-ray radiography

I. Introduction

The use of stainless steel in the power-generation industry had been well documented in the past 20 years [1-3]. Stainless steel was chosen not only for its corrosion-resistant properties but also because it is mechanically suitable for most of the industry's critical components; the turbine system in particular. The geothermal industry has exclusively opted for the use of stainless steel due to the highly corrosive nature of the geothermal steam and the brine that comes with it[4].The material selection process in a geothermal power plant are largely vary based on the steam characteristics and the turbine design, with some selections relied heavily towards one side of the criteria than the others. Most manufacturers are using martensitic stainless steel as the primary material for both rotor and stator blades, while using high strength low-alloy steel for the rotor shaft and disk; particularly ones that incorporated vanadium in their system to increase the material's fatigue limit[5]. AISI 410 and 420 alloys are some of the common blade material options[6], with the likes of AISI 4140 sometimes used for its high corrosion fatigue resistance[7]. However, some cases showed that martensitic stainless steel often suffered damages from excessive stresses that were aided by the erosive nature of the steam and the system vibration[8, 9]. Some findings had also suggested against using martensitic stainless steel where corrosion was the main threat, especially in the presence of higher concentration of CO_2 and H_2S[10] that can lead to a higher probability of stress-corrosion cracking (SCC)[11]. In such cases, precipitation hardened (PH) stainless steel is more preferred, with some on and off-field experiences confirming the effectiveness of it, such as the accelerated corrosion testing in a simulated geothermal environment by Sakai, et al that showed the then newly-developed PH 16Cr-4Ni alloy better SCC resistance than the 13Cr steel[12], or a study of the Hengill geothermal unit by Buzaianu et al, which revealed that no evidence of corrosion was sighted, aside from some apparent depositions, on the surface of the turbine rotors made from 12Cr PH stainless steel, that was inspected during a maintenance period[13].

It was not surprising that stainless steel is still the main choice for many components in geothermal power plants, as well as other energy-producing facilities. This is proven to be a constant challenge for establishing such facilities in countries where domestic stainless steel products are not available. Cheaper imported products have helped manufacturers in these predominantly developing countries to support their geothermal industries but they are not quite enough to significantly reduce the production and distribution cost, or the price of electricity nationally.

ISSN 2278-2540 | DOI: 10.51583/IJLTEMAS | Volume XIII, Issue III, March 2024

With the raise of new method in producing electric steel, like the inductive melting method using the improved inverter technology, it opens up a new possibility for local manufacturers to compete in the power plant components market[14]. A new way of inductive casting from scrap metals in particular has become a trend in more than a decade. The flexibility of using vast selections of material feedstock and controlling the continuous charging without using reductive energy have made this method the staple of many emerging casting industries[15]. It has also been quite successful in promoting the use of scrap steel in recent years, as proved by the increasing number of scrap steel movement over larger manufacturing countries since the 1990s, that leads to better sustainability in the steel manufacturing industries[16].

Technically speaking, the arguably simpler process of re-melting using the inductive melting method and adjusting the composition of the intended alloy from the combined scrap of several alloys followed by the near net shape approach of the investment wax casting, making it such a robust manufacturing technique[17]. This technique has been successfully applied to many industrial component manufacturing processes, like in the production of industrial pumps or valves[18], but seldom in the production of a critical component in demanding working conditions, i.e. turbine blades. Information regarding the resulting products is also very rare, especially from a material standpoint.

This paper will try to explore more about the characteristics of scrap-based, investment-cast products of a 17-4 PH (SUS 630; JIS) alloy. This alloy was chosen not only for its precipitation-hardened nature but also because of its known martensitic structure that resembles the martensitic stainless steel in many power plant's turbine components. The investigation will not include the corrosion resistance properties of this recycled alloy against the geothermal fluids as it will be a subject for another study. Instead, this paper will be focusing more on some of the mechanical features of the alloy and how they are correlated with its microstructures, as well as the casting quality of a turbine blade product made from this alloy in a local manufacturer.

II. Methodology

The casting process was practiced in a smaller setup using the facility of a local manufacturer whose cast product are made daily in the production line. Similar steps and conditions that are used for casting stainless steel product in said manufacturer were also used in the making of the samples. A High frequency induction furnace with a maximum working frequency of 10 kHz and a maximum melting capacity of 300 kg was used for the re-melting and balancing process as may be seen in **Fig.1a**. For efficiency, the maximum melting capacity was met for every run with a maximum of 2.5 to 3 kHz was used per cycle. The building block of this process lied on two types of steel scrap that are popular in many similar producers; the low-alloy steel SPCC (steel plate cold-rolled coiled) that was highly malleable and had very low content of alloying elements as the main part, and the duplex stainless steel S2205 to give a flexible base for stainless-steel-making as a minor addition. Modification process to meet the compositional standard was achieved by adding Ferro-alloy components during the balancing process. Especially for integral elements in stainless steel such as Ni, Cr, Mo, Cu, and Nb. Elemental composition from ASTM 1028-03 (Grade F alloy) [19] was used as designated values to calculate the weight percentages from each available precursor.

As most local manufacturers are working with un-vacuumed setup, so did the work in this paper. Therefore, aside from a strictly controlled and lowly exposed process, batches of deoxidizers were added in the initial melting and during the final step of balancing process, to reduce unnecessary oxidation reactions. Additionally, a set of nozzles were connected to the blowhole beneath the induction chamber to provide a flow of inert gas during the process. The targeted 17-4 PH alloy composition, the SPCC and duplex compositions, the Ferro-alloys compositions, and the deoxidizer's compositions can be found in **Table 1**.as follows.

Table 1. Chemical Composition of Stainless Steel 17-4PHand Casting Materials Used

(a) Targeted Chemical Composition (Standard ASTM A564/A564M)

Komposisi %	SS 17-4PH
Carbon	0,04 - 0,07
Mangan	1 maks
Phospor	0,04 maks
Sulfur	0,03 maks

(b) Casting Material (Scrap)

Casting Material	Volume
2205	80 kg
SPCC	155 kg
Fe Cr HC	-
Fe Cr LC	47,5 kg

(c) Balanced Chemical Composition (Scrap Based)

Komposisi %	SS 17-4PH
Carbon	0,041
Mangan	0,79
Phospor	0,023
Sulfur	0,0103

ISSN 2278-2540 | DOI: 10.51583/IJLTEMAS | Volume XIII, Issue III, March 2024

	Silicon	1 maks	Fe Si	1 kg	Silicon	0,984	
	Nickel	3 - 5	Fe Mn	1 kg	Nickel	4,92	
	Chrom	15 - 17,5	Cu	1 kg	Chrom	16,42	
	Mo	Trace	Fe Ni	11 kg	Mo	0,91	
	Nb	0,15 - 0,45	Nb	3 kg	Nb	0,435	
	Cu	3 - 5			Cu	4,26	

The process is as follows. In the first step of charging, 25%of the furnace was filled with only SPCC and duplex scraps. The melting process started gradually until the inside of the chamber reached 1500 °C. Both scraps were expected to be fully melted and stabilized in around 60 minutes since the process was run "clean" (no return scrap was used). Nevertheless, deoxidizers in the form of Ferro-silicon (Fe-Si) and Ferro-manganese (Fe-Mn) were added to help speed up the process. Ferro-chromium (Fe-Cr), Ferro-nickel (Fe-Ni), and Ferro-copper (Fe-Cu) alloying compounds were then added subsequently. The remaining SPCC and duplex scraps were placed into the mix after 10-15 minutes and then held at a temperature slightly above 1600 °C for 30 minutes. After that, the heater was switched off, allowing the batch to cool down while ferro-niobium (Fe-Nb) compound was added into the system. Although it is not one of the element that was listed in the standard, the addition of Niobium was deemed necessary to assist the formation of intermetallic constituent as a possible nucleation site for precipitation and lowering the elastic deformation energy of the lattice during precipitation period[20]. Especially, since the nature of the parent metal itself was not of a precipitation-hardening steel. Cleaning was performed by the aid of slag catcher powder. After the first cleaning step, the heat was switched off and calcium-silicon (Ca-Si) compound was added to the mix as the last deoxidizer. Once the temperature was measured at around 1400 °C, Argon gas (97% purity, Samator) stream entered the chamber with a flow of 2 L/minute for 3 minutes. The process was finished by the second cleaning step using the same type of slag catcher powder.

(a) 300 kg capacityhigh frequency induction furnace (b) Pouring of scrap-based molten 17-4 PH

Figure 1(a,b) High frequency induction furnace used and pouring of scrap-based molten Steel into the investment wax-lost casting into the investment wax-lost casting

A small sampling of molten metal was taken for a compositional check before the final stage. The test was performed in a solid state using Foundry-Master Pro optical emission spectrometer (Oxford Instruments), to check the accuracy of every element in refer to the material target. A 3% difference (1% for some crucial elements) would trigger a secondary check procedure from the same batch. If the difference persisted, the balancing process would continue until the composition matched the target in **Table**

ISSN 2278-2540 | DOI: 10.51583/IJLTEMAS | Volume XIII, Issue III, March 2024

1. The final composition of the scrap-based 17-4 PH alloy can also be found in the same table.

The investment casting mold was made by dipping the wax-shaped design, which was first cast in an aluminum dies, into a ceramic slurry consisted mainly of zirconium flour, colloidal silica, and mullite, with a coated zirconia sand on the outer layer of the mold. The mold was sintered and pre-heated prior of use. The 17-4 PH batch was poured into the mold at around 1550 °C to ensure the stability of the molten phase. In this work (**Figure 1b.**), the mold was designed to be very thin (less than 0.5 mm wall thickness) to accommodate the solidification rate of a martensitic-type stainless steel as well as providing better flow-ability inside the mold. The casting results were taken out from the mold after they reached temperature below 100 °C. An example of the blade prototype (stage 6) after finishing can be seen in **Figure 2 (a)**, following the design drawing in **Figure2(b)**.

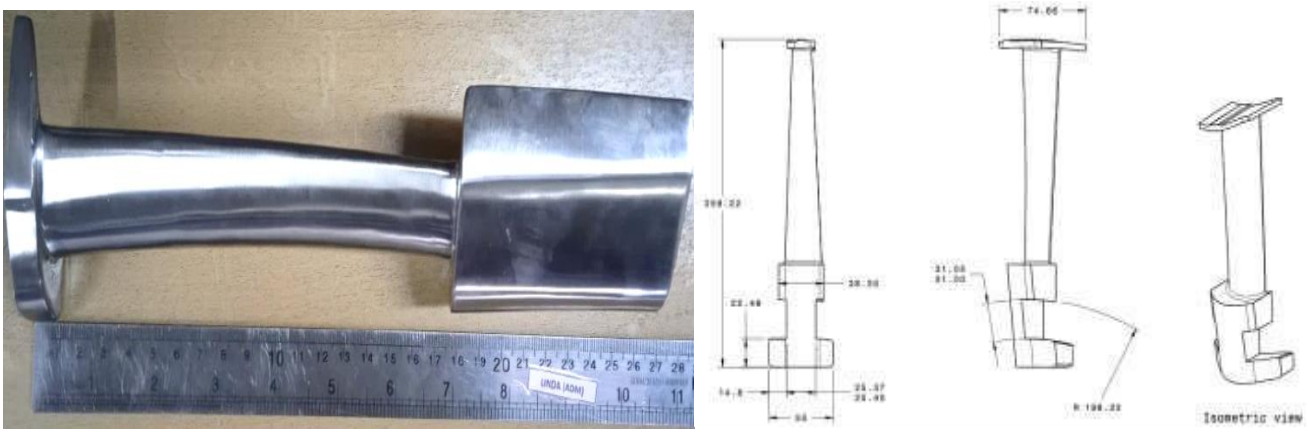

(a) Prototype of the Turbine Blade Stage No. 3 (b) Design of the Turbine Blade Stage No.3

Figure 2. Prototype and Design of the Rotor Turbine Blade No.3 Stage

To check the integrity of the casting process, single wall imaging x-ray radiography was performed on finished blade prototypes stage 1 and 6 using HD CR 35 NDT (Duer) with 150 kV of working tube voltage and a source-to-film distance of 600 mm. The scan rate of 300 rpm was applied to each side of the blade. Some part of the stage 6 blade prototype was deemed too thick for a single capture, thus, images from each side were taken separately with varied exposure times (6 to 20 s).

In addition to the prototypes, several samples were purposefully made to investigate the material further. These samples were heat treated to induce precipitation hardening, according to the program listed in **Table 2**. HTC 03/15 C450 muffle furnace (Naber therm) with SiC rods heating elements under Nitrogen environment (99.99% purity, Sama tor) was used for all treatments involved, aside from the cooling process. All samples endured homogenizing at 1180 °C and furnace cooled up to 24 h, followed by austenizing at around 1050 °C. 5 samples were subjected to aging treatment at various temperatures and 1 sample was kept as control. All samples were cooled at room temperature after austenizing and aging treatments. A commercial 17-4 PH and an as-cast samples were used as points of reference.

Uniaxial tensile test of the samples was done using AGX250kN universal testing machine (Shimadzu) with a speed of test of 0.5 mm/minutes on tubular tensile specimens, in accordance to ASTM E8/E8M-13. The yield stress, ultimate tensile stress, and total elongation were all recorded. Dura Scan automatic tester (Struers) in the micro Vickers mode on a 1 kg f load setting was used to measure hardness. The hardness number of each specimen is the average value of 5 indentations taken diagonally across the specimen's surface.

Microstructure samples were prepared by grinding and polishing until they reached mirror-like finish. Etching was done in 2 steps in a specific manner that was developed to match the challenge when etching with remelted products. The first step was done by applying Kalling's no.2 for 120 to 240 s at room temperature to reveal the development of the martensitic structure and the appearance of δ-ferrite in the annealed state. The second step was a selective etching method by applying murakami's reagent and modified murakami's reagent [21] at 120 s each with a cleaning interval of 60 s between each treatment. This process was preferred to highlight δ-ferrite formation and distribution after each aging stage. The second consecutive etching was also important to give extra attention towards the secondary phases that otherwise would not be apparent in the first etching, e.g. metallic carbides formation, σ phase, and others. Microstructural observation was mainly done using VX1000 laser confocal microscope (Keyence) using both visible light and laser from light source. JIB-4610F field emission-scanning electron

ISSN 2278-2540 | DOI: 10.51583/IJLTEMAS | Volume XIII, Issue III, March 2024

microscope (FE-SEM) equipped with EDS (JEOL) was also utilized to check the actual position of the secondary phases, and more importantly the size, composition, and location of the precipitated particles from the annealed samples.

In addition to the prototypes, several samples were purposefully made to investigate the material further. These samples were heat treated to induce precipitation hardening, according to the program listed in **Table 2**. HTC 03/15 C450 muffle furnace (Naber therm) with Si C rods heating elements under Nitrogen environment (99.99% purity, Samator) was used for all treatments involved, aside from the cooling process. All samples endured homogenizing at 1180 °C and furnace cooled up to 24 h, followed by austenizing at around 1050 °C. 5 samples were subjected to aging treatment at various temperatures and 1 sample was kept as control. All samples were cooled at room temperature after austenizing and aging treatments. A commercial 17-4 PH and an as-cast samples were used as points of reference. Uniaxial tensile test of the samples was done using AGX250kN universal testing machine (Shimadzu) with a speed of test of 0.5 mm/minutes on tubular tensile specimens, in accordance to ASTM E8/E8M-13. The yield stress, ultimate tensile stress, and total elongation were all recorded. DuraScan automatic tester (Struers) in the micro-Vickers mode on a 1 kgf load setting was used to measure hardness. The hardness number of each specimen is the average value of 5 indentations taken diagonally across the specimen's surface.

Microstructure samples were prepared by grinding and polishing until they reached mirror-like finish. Etching was done in 2 steps in a specific manner that was developed to match the challenge when etching with re-melted products. The first step was done by applying Kalling's no.2 for 120 to 240 s at room temperature to reveal the development of the martensitic structure and the appearance of δ-ferrite in the annealed state. The second step was a selective etching method by applying Murakami's reagent and modified Murakami's reagent [21] at 120 s each with a cleaning interval of 60 s between each treatment. This process was preferred to highlight δ-ferrite formation and distribution after each aging stage. The second consecutive etching was also important to give extra attention towards the secondary phases that otherwise would not be apparent in the first etching, e.g. metallic carbides formation, σ phase, and others. Microstructural observation was mainly done using VX1000 laser confocal microscope (Keyence) using both visible light and laser from light source. JIB-4610F field emission-scanning electron microscope (FE-SEM) equipped with EDS (JEOL) was also utilized to check the actual position of the secondary phases, and more importantly the size, composition, and location of the precipitated particles from the annealed samples. In addition to the prototypes, several samples were purposefully made to investigate the material further. These samples were heat treated to induce precipitation hardening, according to the program listed in **Table 2**. HTC 03/15 C450 muffle furnace (Nabertherm) with SiC rods heating elements under Nitrogen environment (99.99% purity, Samator) was used for all treatments involved, aside from the cooling process. All samples endured homogenizing at 1180 °C and furnace cooled up to 24 h, followed by austenizing at around 1050 °C. 5 samples were subjected to aging treatment at various temperatures and 1 sample was kept as a control. All samples were cooled at room temperature after austenizing and aging treatments. A commercial 17-4 PH and an as-cast samples were used as points of reference.

Uniaxial tensile test of the samples was done using AGX250kN universal testing machine (Shimadzu) with a speed of test of 0.5 mm/minutes on tubular tensile specimens, in accordance to ASTM E8/E8M-13. The yield stress, ultimate tensile stress, and total elongation were all recorded. DuraScan automatic tester (Struers) in the micro Vickers mode on a 1 kgf load setting was used to measure hardness. The hardness number of each specimen is the average value of 5 indentations taken diagonally across the specimen's surface.

Microstructure samples were prepared by grinding and polishing until they reached mirror-like finish. Etching was done in 2 steps in a specific manner that was developed to match the challenge when etching with re-melted products. The first step was done by applying Kalling's no.2 for 120 to 240 s at room temperature to reveal the development of the martensitic structure and the appearance of δ-ferrite in the annealed state. The second step was a selective etching method by applying Murakami's reagent and modified Murakami's reagent [21] at 120 s each with a cleaning interval of 60 s between each treatment. This process was preferred to highlight δ-ferrite formation and distribution after each aging stage. The second consecutive etching was also important to give extra attention towards the secondary phases that otherwise would not be apparent in the first etching, e.g. metallic carbides formation, σ phase, and others. Microstructural observation was mainly done using the VX1000 laser confocal microscope (Keyence) using both visible light and laser from light source. JIB-4610F field emission-scanning electron microscope (FE-SEM) equipped with EDS (JEOL) was also utilized to check the actual position of the secondary phases, and more importantly the size, composition, and location of the precipitated particles from the annealed samples.

The heat treatment scheme for 6(six) types of sample coded in A, B, C, D, E and F is depicted in Table 2. As seen in Table 2, the heat treatment proses that carried out in the samples consists of homogenizing, normalizing, austenizing, aging and quenching

ISSN 2278-2540 | DOI: 10.51583/IJLTEMAS | Volume XIII, Issue III, March 2024

processes.

Table 2. Heat treatment schemes for all samples

	Samples					
Treatment	A	B	C	D	E	F
Homogenizing	at 1180 °C for 2 h					
Normalizing	inside furnace until 60 °C					
Austenizing (A)	at 1050 °C for 1 h					
Aging (AG)	-	at 480 °C for 1 h	at 580 °C for 2 h	at 580 °C for 4 h	at 620 °C for 4 h	at 620 °C for 4 h at 760 °C for 2 h
Quenching	after A; at room temperature	after AG; at room temperature				

In this work, X-ray radiography is carried out to inspect the quality of the scrap-based investment-casting of turbine blades 17-4 PH stainless steel rotor blade components. X-ray radiography plays a crucial role in inspecting investment cast metallic alloy products with meticulous detail. In the context of metallic alloy investment casting, the process involves creating intricate shapes by pouring molten metal into a ceramic mold. Typical results obtained through X-ray radiography are as follows

(a) Porosity Detection: X-ray radiography can identify internal porosity within the metallic structure. Porosity appears as dark regions on the X-ray image, helping inspectors assess the quality of the casting by evaluating the density and distribution of these voids.

(b) Crack Identification: Radiography enables the detection of cracks or fissures within the metallic alloy. Even tiny fractures that may not be visible externally can be identified through X-ray imaging, ensuring the structural integrity of the final product.

(c) Wall Thickness Assessment: X-rays allow for precise measurement of wall thickness in different sections of the cast product. This is crucial for ensuring uniformity and compliance with design specifications, as deviations in thickness can impact the mechanical properties of the alloy.

(d) Inclusion Detection: X-ray radiography can reveal any foreign inclusions, such as non-metallic particles or impurities, within the cast structure. Identifying and addressing these inclusions is essential for maintaining the material's integrity and preventing potential weaknesses.

(e) Dimensional Accuracy: By capturing detailed internal features, X-ray radiography aids in verifying the dimensional accuracy of the cast product. This is vital for meeting precise engineering requirements and ensuring the functionality of the final metallic alloy component.

(f) Quality Assurance: The comprehensive imaging provided by X-ray radiography supports thorough quality assurance processes. Inspectors can scrutinize the X-ray images for any irregularities, allowing for early detection and rectification of issues before the product reaches its final stages.

(g) Process Optimization: X-ray radiography not only serves as a quality control tool but also facilitates process optimization. Continuous monitoring through radiographic inspection helps manufacturers refine their casting techniques, enhancing overall efficiency and minimizing the likelihood of defects.

The results of X-ray Radiography for rotor blade prototype stage no.1 and no.6 may be seen in Figure 3.

ISSN 2278-2540 | DOI: 10.51583/IJLTEMAS | Volume XIII, Issue III, March 2024

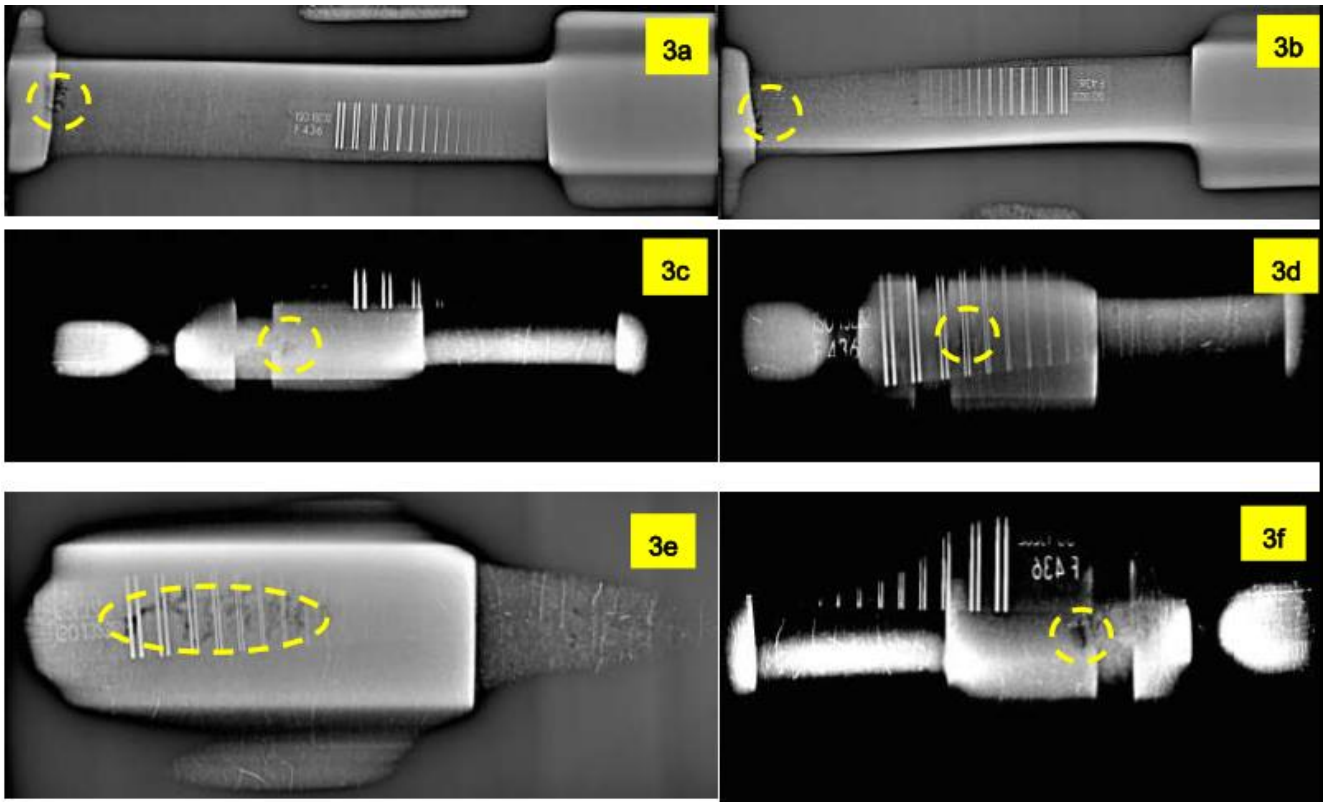

Figure 3. X-Ray Radiography Results of blade prototype stage 1 and 6. From top left: 3a. stage 6 front side; 3b. stage 6 back side; 3c. stage 1 front side; 3d. stage 1 back side; 3e. stage 6 diaphragm-side prolonged view; 3f. stage 1 prolonged view

The characterization of the mechanical properties of 17 4PH alloys were carried out using the uniaxial tensile test using AGX250kN universal testing machine (Shimadzu). In this work, 8 (eight) types of samples were attempted to evaluate mechanical properties obtained, as seen in Figure 4 and the types of sample are depicted in Table 2.

Table 2. Type of Tensile Test Sample

No	Type of Sample	Heat Treatment			Yield Stress (MPa.)	Ultimate Tensile Stress (MPa.)	Elongation (%)
		Austenizing	Precipitation Hardening	Quenching			
1	As-Cast	No heat treatment	No	Air quench	677.46	676.74	9.33
2	Sample A	1050 deg C, 30 minutes	No	Air quench	1033.33	1017,50	2.50
3	Sample B	1050 deg C, 30 menit	No	Room Cooling	993.83	985,82	3.00
4	Sample C	1050 deg C, 30 menit	480deg C, 1 hour	Room Cooling	995.25	966,34	2.86
5	Sample D	1050 deg C, 30 menit	580 deg C, 2 hours	Room Cooling	894.17	742	3.45
6	Sample E	1050 deg C,	580 deg. C, 4	Room	841.91	711.01	3.48

ISSN 2278-2540 | DOI: 10.51583/IJLTEMAS | Volume XIII, Issue III, March 2024

		30 menit	hours	Cooling			
7	Sample F	1050 deg C, 30 menit	620 deg C, 4 hours	Room Cooling	533.69	447,82	8.13
8	Commercial Product	Not Available	Not Available	Not Available	740.00	1070.00	16

Uniaxial tensile tests measure a material's response to stretching forces. Different heat treatments can influence the mechanical properties. Generally, increasing heat treatment temperature or duration can affect tensile elongation (TE), yield stress (YS), and ultimate tensile stress (UTS). Some of heat treatment processes that could influence the mehanical properties are as follows:

(a) Annealing: Higher temperatures or extended durations often result in increased elongation and reduced yield stress. This is due to recrystallization and grain growth, making the material more ductile.

(b) Quenching: Rapid cooling after heating can lead to increased yield stress and ultimate tensile stress but decreased elongation. This is because quenching produces a harder and more brittle microstructure, enhancing strength at the expense of ductility.

(c) Tempering: Controlled heating and cooling can balance strength and ductility. Tempering typically results in a moderate increase in yield stress, a reduction in ultimate tensile stress, and an improvement in elongation compared to quenched states.

Understanding the trade-offs between these properties is crucial for selecting the appropriate heat treatment based on the desired mechanical characteristics for a specific application.

The uniaxial tensile test results obtained in this work are depicted in Figure 4.

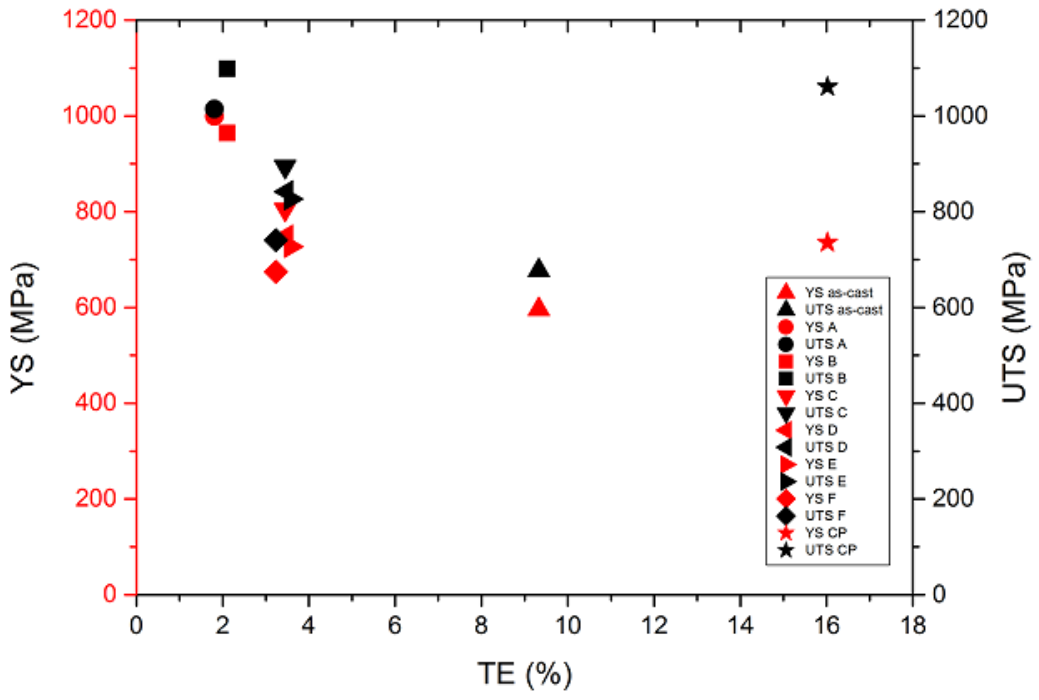

Figure 4. Tensile test results of all samples, including an as-cast product and a commercially 17-4 PH

As seen in Figure 4, the tensile elongation (TE) and yield strength (YS) are related in materials' mechanical behavior. Yield strength represents the point at which a material undergoes plastic deformation, while tensile elongation measures the material's ability to stretch before breaking. Generally, materials with higher yield strength tend to have lower tensile elongation, indicating

ISSN 2278-2540 | DOI: 10.51583/IJLTEMAS | Volume XIII, Issue III, March 2024

they are less ductile. Conversely, lower yield strength often correlates with higher tensile elongation, signifying greater ductility. The relationship varies depending on the material's composition and structural properties.

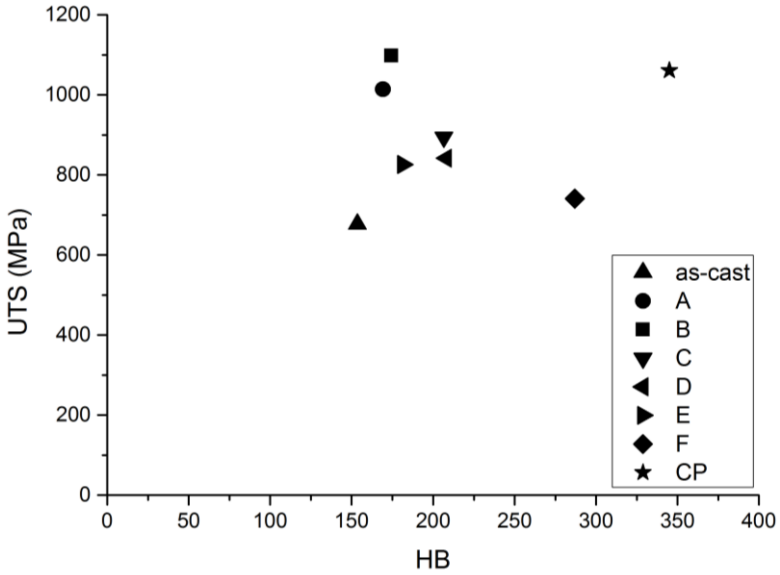

Figure 5. A correlation between the strength of all samples with their Brinell hardness numbers

The relationship between ultimate tensile strength (UTS) and Brinellhardness (HB) of a material is not straightforward, as they represent different mechanical properties, as may be seen in Figure 5. Ultimate tensile strength (UTS) measures the maximum stress a material can withstand under tension, while Brinell hardness (HB) indicates a material's resistance to indentation. However, in some cases, there might be a correlation between hardness and tensile strength, especially in materials with similar microstructures. For example, harder materials may generally exhibit higher tensile strength due to their ability to resist deformation. Keep in mind that the correlation can vary based on factors such as alloy composition and heat treatment.

III. Results and Discussion

X-Ray radiographic images reveal casting defects on both stage number 1 and stage number 6 of the blade prototypes, as seen in **Figure 3**. Figure 3(a) and Figure 3(b) show a crack-like discontinuities on the shaft-end of the stage number 6 blade, marked by the yellow dash-circles, on both sides of the same place after 8 seconds of exposure. Given that half of the defects are transparent enough on Fig. 3a but not on Fig 3b, it can be assumed that the defects lies in line with the thinner part of the blade body. Both figures also show an almost identical clarity and shape of the defects which suggest that these defects are the same, occupying a significant portion of the thickness in the thinner part. This kind of defect often appears on a gravity-type casting where discrepancies of flow in the filling process leads to shrinkage-related porosity[18]. This kind of knowledge is well-known to many casting industries, but nevertheless, achieving full control of the material flow remains impossible in this type of casting process.

The observation on the prototype of turbine blade stage No. 1 shows a rather similar behavior to the stage no. 6 rotor blade where a single defect is quite apparent within the same exposure period, as seen in Figure 3(c)and Figure 3(d.). Despite, it is almost 3 times shorter than that of the stage No. 6 blade, the casting of the stage No.1 blade was still affected by the incomplete flow through its thicker part. However, with such shape of defect, we might assume that rather than shrinkage problem, the flow ability of the material itself as a result of an increased density during the last step of, the segregation of alloying element(s), i.e. in this case, it is due to a somewhat higher Cu content, or a void left by reacting gases is a more likely culprit. The defect image in Figure 3(c) is found relatively very thin compared the other defects.

IV. Conclusions

As a general conclusion, the strategy that can be adopted to recycle metal scrap into stainless steel alloys, by following these detailed steps, you can effectively recycle metal scrap into high-quality stainless steel alloys.as follows:

(a) Collection and Sorting

ISSN 2278-2540 | DOI: 10.51583/IJLTEMAS | Volume XIII, Issue III, March 2024

- Collect metal scrap from various sources, including industrial waste, consumer products, and demolition.
- Sort the scrap based on metal types to ensure a homogeneous feedstock for the recycling process.

(b) Preparation for Melting

- Remove non-metallic contaminants like coatings, paints, and insulation from the scrap.
- Cut or shred large pieces into smaller, manageable sizes to facilitate melting.

(c) Melting

- Use an electric arc furnace or induction furnace to melt the prepared metal scrap.
- Adjust furnace temperature and atmosphere to melt the metal while minimizing oxidation and maintaining energy efficiency.

(d) Separation of Impurities

- Employ fluxes or other refining agents to remove impurities such as sulfur, phosphorus, and unwanted alloys.
- Adjust the chemical composition by adding alloying elements like chromium, nickel, and manganese to achieve the desired stainless steel composition.

(e) Refining Process

- Refine the molten metal to improve its cleanliness and consistency.
- Utilize processes like argon oxygen decarburization (AOD) or vacuum oxygen decarburization (VOD) to reduce carbon content and enhance stainless steel properties.

(f) Casting

- Cast the refined molten metal into semi-finished forms such as ingots or slabs.
- Control casting parameters to ensure the desired structure and properties in the final stainless steel product.

(g) Heat Treatment

- Subject the cast stainless steel to heat treatment processes like annealing, quenching, and tempering to achieve the desired mechanical properties.
- Control heating and cooling rates to optimize the microstructure.

(h) Cold Working

- Employ processes like rolling, forging, or drawing to further shape and refine the stainless steel
- Cold working enhances strength and toughness while improving surface finish.

(i) Finishing Processes

- Apply surface treatments, such as pickling or passivation, to remove oxides and enhance corrosion resistance.
- Cut, grind, or polish the stainless steel to meet specific dimensional and aesthetic requirements.

(j) Quality Control

- Implement rigorous quality control measures throughout the entire recycling and manufacturing process.
- Use testing methods like spectroscopy, metallography, and mechanical testing to ensure the stainless steel meets industry standards.

(k) Environmental Considerations

- Optimize recycling processes to minimize energy consumption and emissions.
- Implement eco-friendly practices to reduce the environmental impact of stainless steel production.

ISSN 2278-2540 | DOI: 10.51583/IJLTEMAS | Volume XIII, Issue III, March 2024

The work carried out herein has shown a strategy of the general steps involved in recycling metal scrap to manufacture stainless steel 17-4PH turbine blades. It's important to follow strict quality control and metallurgical standards to produce high-quality material that meets industry specifications.

Recycling metal scrap into stainless steel alloys, i.e. Stainless Steel 17-4PH, involves several key steps. Firstly, collect and sort the scrap based on metal types. Then, melt the scrap in a furnace, adjusting temperatures to separate impurities. Add alloying elements like chromium and nickel to achieve stainless steel composition. Refine the mixture, cast it into desired shapes, and heat treat for strength. Finally, cold working and finishing processes enhance the alloy's properties. Ensure strict quality control throughout to produce high-quality stainless steel from recycled metal.

Acknowledgements

The authors gratefully acknowledge the financial support provided from the LPDP funding, through the Decree from The Deputy for Research and Innovation Facilitation No. 60/II/HK/2022 administered by the National Research and Innovation Agency (BRIN), Republic of Indonesia.

Conflict of Interest

The authors declare no conflict of interest.

References

1. D. Gooch, International materials reviews, 45 (2000) 1-14.
2. A. Sakuma, T. Matsuura, T. Suzuki, O. Watanabe, M. Fukuda, JSME International Journal Series B Fluids and Thermal Engineering, 49 (2006) 186-191.
3. M. Zhu, Journal of Physics: Conference Series, IOP Publishing, 2019, pp. 012056.
4. T. Kaya, P. Hohan, P. Corrosion, 2005.
5. Y. Sakai, Y. Oka, H. Kato, Fuji Electronic Review, 55 (2008) 87-92.
6. Y. Sakai, K. Nakamura, K. Shiokawa, Fuji Electronic Review, 51 (2005) 90-95.
7. B. Boardman, ASM International, Metals Handbook. Tenth Edition, 1 (1990) 673-688.
8. Z. Mazur, R. García-Illescas, J. Porcayo-Calderón, Engineering Failure Analysis, 16 (2009) 1020-1032.
9. J. Kubiak, J. González, F. Sierra, J. García, J. Nebradt, V. Salinas, Journal of failure analysis and prevention, 5 (2005) 26-32.
10. K.A. Lichti, Materials at high temperatures, 24 (2007) 351-363.
11. L. Wu, Y. Takeda, H. Morita, T. Shoji, Corrosion, 73 (2017) 125-137.
12. Y. Sakai, M. Yamashita, K. Shiokawa, L.B. Niu, H. Takaku, The Proceedings of the International Conference on Power Engineering (ICOPE) 2003.3, The Japan Society of Mechanical Engineers, 2003, pp. 3-297-293-302_.
13. A. Buzăianu, I. Csaki, P. Moţoiu, K. Leósson, S. Serghiuţă, A. Arnbjornsson, V. Moţoiu, G. Popescu, S. Guðlaugsson, D. Guðmundsson, IOP Conference Series: Materials Science and Engineering, IOP Publishing, 2016, pp. 012043.
14. M. Chaabet, heat processing, 10 (2012) 49-58.
15. T. Manabe, M. Miyata, K. Ohnuki, Journal of Sustainable Metallurgy, 5 (2019) 319-330.
16. H. Lee, I. Sohn, Journal of Sustainable Metallurgy, 1 (2015) 39-52.
17. W. Ertl, E. Dötsch, 2015.
18. P.-H. Huang, M.-J. Guo, Materials Research Innovations, 19 (2015) S9-77-S79-81.
19. ASTM, A1028-03, ASTM International, United States, 2015, pp. 4.
20. F. Mariani, G. Takeya, L.C. Casteletti, A.L. Neto, G. Totten, Materials Performance and Characterization, 5 (2015) 38-46.
21. Pace Technologies, Safety Data Sheet of Murakami's Reagent, Pace Technologies, Tucson, Arizona, USA (2023).